ac conductivity in a DNA charge transport model

P. Maniadis,[1] G. Kalosakas,[1] K. Ø. Rasmussen,[2] and A. R. Bishop[2]
[1]*Max Planck Institute for the Physics of Complex Systems, Nöthnitzer Str. 38, D-01187 Dresden, Germany*
[2]*Theoretical Division and Center for Nonlinear Studies, Los Alamos National Laboratory, Los Alamos, New Mexico 87545, USA*
(Received 12 April 2005; published 29 August 2005)

We present the ac response of a DNA charge transport model, where the charge in the π-stack interacts with the base-pair opening dynamics of the double strand. The calculated ac conductivity exhibits prominent peaks at polaron normal modes with electronic character, while weaker response appears at lower frequencies in the vibrational part of the polaron normal mode spectrum. Examples of the former, strong peaks, show redshifts as the amplitude of the ac field increases.

DOI: 10.1103/PhysRevE.72.021912 PACS number(s): 87.15.Aa, 78.67.−n, 63.22.+m

The electronic conduction properties of DNA have recently attracted much attention both among biologists and physicists. There is clear evidence that charge injection and migration is associated with damage, mutation, and repair of DNA [1], and excitement has been generated by the emergent nanotechnology aspects of single molecule DNA conduction [2–4]. The basis for the potential single molecule conduction is rooted in the unique structure of DNA resulting in orderly π-π orbital stacking with 3.4 Å separation, which resembles a high mobility structural pathway for charge transfer. This supposed π-way was initially referred to as "wirelike," however much controversy surrounds the understanding of the nature of the measured charge transport along the double helix. This is the consequence of conflicting experimental reports that range from suggesting DNA to be metallic [5], to semiconducting [6], and insulating [7].

In this controversy the detailed dc transport measurements performed by Yoo *et al.* [8] stand out because these results are well explained by a model in which the conduction is due to thermally activated hopping of small polarons [9]. Further evidence for the small polaron mechanism is provided by recent *ab initio* calculations [10], demonstrating a strong hole-lattice coupling and clear evidence for the formation of small polarons in DNA. This work also demonstrated that the large deformation of the macromolecule resulting from polaron formation occurs at the weakest bonds in the base-pair complex. The weakest bonds are clearly the two (*AT* base pairs) or three (*GC* base pairs) hydrogen bonds forming between the complementary bases in the double helix. The most important structural degrees of freedom in this context is therefore the hydrogen bonds between complementary bases.

Several microscopic polaronic models, which take into account the coupling of a charge carrier in a DNA helix with the structural degrees of freedom of the deformable biomolecule have been proposed [11–17]. Here, we will take advantage of the accurate description of the base-pair dynamics [18–20] provided by the Peyrard-Bishop-Dauxois (PBD) model [21]. This model has, by detailed comparison to several experiments, been demonstrated to describe very accurately the dynamics of the strand separation in double stranded DNA. In agreement with the findings of *ab initio* calculations [10], we have previously proposed the coupling of the charge's on-site energy—in a tight-binding framework—with these structural motions, in order to explore polaronic effects [13–15].

Here, we are mainly interested in the behavior of the ac conductivity of the coupled model. Contactless ac conduction measurements have been performed, investigating both the temperature [22] and the frequency dependence of the ac conductivity [23,24]. The temperature dependence has been theoretically discussed in several studies [25,26]. The measured variation of the conductivity with frequency shows a power law dependence below ~1 THz [23,24]. Although it has been argued that the observed ac conductivity at low frequencies is most likely due to dissipation from dipole motion in the water surrounding the helix [24], there is likely to also be some absorption due to doping at DNA breaks [27]. Even though other factors may be dominating the optical response at lower frequencies, important signatures of polarons can exist at higher frequencies. We therefore calculate the frequency dependence of the real and imaginary part of the ac conductivity of the model at relatively higher frequencies and zero temperature. We have previously determined [14] the detailed polaron normal mode spectrum of the model we are applying. This normal mode spectrum will be crucial for our understanding of the features we observe in the ac conductivity. Due to the dominant effects of the trapped water or doping at lower frequencies [24,27], we do not expect our present model to reproduce experimental observations in the low frequency regime (below ~1 THz).

In the semiclassical approximation [13–15], the equations of motion of this model, in the presence of an electric field $E(t)$, read

$$i\hbar\frac{d\Psi_n}{dt} = -V(\Psi_{n+1}+\Psi_{n-1}) + \chi y_n \Psi_n - q_e n d E(t)\Psi_n \quad (1)$$

and

$$m\frac{d^2y_n}{dt^2} = -V_M'(y_n) - W'(y_n,y_{n-1}) - W'(y_{n+1},y_n) - \chi|\Psi_n|^2 - m\gamma\frac{dy_n}{dt}, \quad (2)$$

where n labels the base pairs along a DNA chain, Ψ_n is the probability amplitude for the charge carrier located at the nth

base pair, y_n corresponds to the stretching displacement of the nth base pair from equilibrium, q_e is the carrier's charge, $d=3.4$ Å is the distance between successive base pairs, χ is the charge-vibrational coupling constant, V is the tight-binding hopping integral taken equal to 0.1 eV, and V_M, W are the on-site and stacking potential energies, respectively, of the PBD model,

$$V_M(y_n) = D(e^{-ay_n} - 1)^2, \tag{3}$$

$$W(y_n, y_{n-1}) = \frac{k}{2}(1 + \rho e^{-\beta(y_n + y_{n-1})})(y_n - y_{n-1})^2. \tag{4}$$

In Eq. (2), $m=300$ amu is the nucleotide mass, prime denotes differentiation with respect to y_n, and the last term represents the dissipation necessary for achieving a steady state under the action of a periodic external field $E(t)$. The parameters of the PBD potentials (3) and (4) are $D=0.04$ eV, $a=4.45$ Å^{-1}, $k=0.04$ eV/Å^2, $\rho=0.5$, and $\beta=0.35$ Å^{-1} [21]. We have considered the case of homopolymer DNA and a length of $N=100$ base pairs in our numerical calculations. For more details about the coupled charge-vibrational model see Refs. [13–15].

This model admits polaronic solutions as ground states and here we consider their response to an external ac electric field. The optical conductivity is obtained through numerical calculation of the current density, when a steady state is reached in the presence of the periodic external perturbation. In our discrete system the local current density at the nth base pair is

$$J_n(t) = \frac{i\hbar q_e}{2m_e d^2}[\Psi_n(\Psi^*_{n+1} - \Psi^*_{n-1}) - \Psi^*_n(\Psi_{n+1} - \Psi_{n-1})], \tag{5}$$

while the average current density through the one-dimensional stack is given by

$$J(t) = \frac{1}{N}\sum_{n=1}^{N} J_n = \frac{\hbar q_e}{m_e L d}\sum_{n=1}^{N} \mathrm{Im}[\Psi^*_n(\Psi_{n+1} - \Psi_{n-1})], \tag{6}$$

where m_e is the mass of the carrier, N is the total number of base pairs, and $L=Nd$ the length of the considered DNA.

In linear response, the optical conductivity $\sigma(\omega)$ is derived in the steady state from the proportionality relation between the current density and the electric field in the frequency domain,

$$J(\omega) = \sigma(\omega)E(\omega). \tag{7}$$

The initial state for our simulations is the ground state polaron. We solve numerically the equations of motion (1) and (2) in the presence of an ac electric field,

$$E(t) = E_0 \cos(\omega t). \tag{8}$$

After an initial transient time, the system reaches a steady state, where the current density is

$$J(t) = J_0 \cos(\omega t + \phi). \tag{9}$$

From the Fourier transform of $J(t)$ and $E(t)$, using Eq. (7) we obtain the real and imaginary part of the ac conductivity as

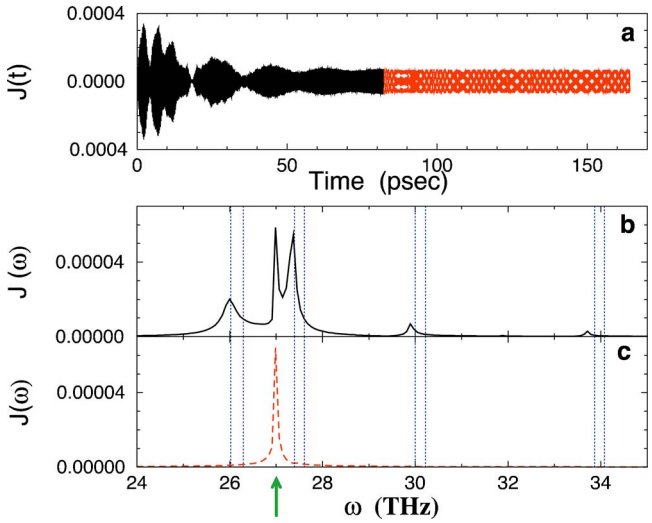

FIG. 1. (Color online) (a) Current density $J(t)$ in arbitrary units as a function of time for $\chi=0.6$ eV/Å, $E_0=2\times10^{-6}$ V/Å, and driving frequency $\omega=27$ THz. Continuous line (left part) corresponds to the transient behavior and dashed line (right part) to the steady state. (b) and (c) Fourier transforms of the transient and the steady state, respectively. The vertical dotted lines in (b) and (c) show positions of the polaronic normal mode frequencies. The arrow in the x axis in (c) indicates the frequency of the electric field applied.

$$\sigma(\omega) = \frac{J_0}{E_0}e^{-i\phi}. \tag{10}$$

Varying the frequency ω of the external field (driving frequency), we calculate the dependence of $\sigma(\omega)$.

In Fig. 1(a) we show the typical behavior of the current density $J(t)$, Eq. (6), found in our simulations. The left part of the curve (continuous line) corresponds to the initial transient behavior, and the right part (dashed line) to the steady state. The corresponding Fourier transforms of these two regimes are shown in Figs. 1(b) and 1(c), respectively. In Fig. 1(b), apart from a strong signal response at the driving frequency, additional peaks exist in the Fourier transform of the transient regime, corresponding to excited internal modes. In the steady state the internal modes have been damped and only the driving frequency remains. The friction parameter γ is modified during the numerical simulations in order to accelerate the relaxation process and more rapidly eliminate the transient behavior of the system. We start with $\gamma=10$ ps^{-1} and then we gradually decrease it in small steps (in order to avoid additional transient behavior) to the final value $\gamma=2$ ps^{-1}. We have chosen this final value so as to produce a peak sufficiently broad to be observed within the resolution of the frequency increments we use in order to cover an extended regime in ω.

In Fig. 2 we present the dependence of the real part (σ_R) and the imaginary part (σ_I) of the ac conductivity on the frequency of the external field. The optical conductivity exhibits strong peaks at resonances with normal modes of the polaron. The positions of the frequencies of the polaron's normal modes are also shown in Fig. 2 by vertical dotted lines. A detailed investigation of the polaron eigenmodes and

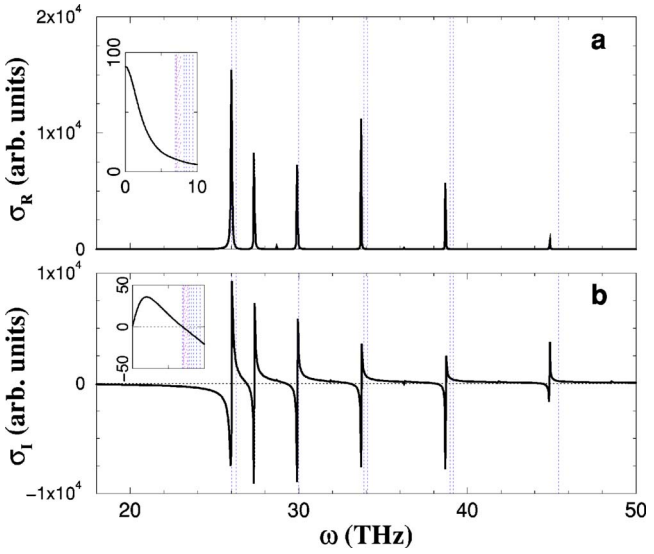

FIG. 2. (Color online) (a) Real part σ_R and (b) imaginary part σ_I of the conductivity as a function of frequency, for $\chi=0.6$ eV/Å and $E_0=2\times10^{-8}$ V/Å. In the insets we plot the real and imaginary parts, respectively, of the conductivity for low frequencies, i.e., in the vibrational part of the spectrum. Vertical dotted lines show the positions of normal mode frequencies of the polaron, while the shadowed stripe in the insets represents the phononic band.The dotted horizontal line in (b) indicates the zero value.

their dependence on the coupling parameter χ has been presented in Ref. [14]. The strongest peak in the conductivity occurs at the lowest frequency polaronic normal mode with primarily electronic character (see Ref. [14]), with frequency $\omega_{e1}=26.019$ THz for the case of $\chi=0.6$ eV/Å, shown in Fig. 2. The polaronic normal modes appear in adjacent pairs of even and odd symmetry. Only the antisymmetric modes are observed to respond to the ac drive. In addition to the prominent features in $\sigma(\omega)$ at the electronic part of the polaron normal mode spectrum (at relatively high frequencies), the system exhibits weaker response in the vibrational (phononic) part of the spectrum at lower frequencies (see insets of Fig. 2). In this regime, for $\chi=0.6$ eV/Å there is an antisymmetric pinning mode with vanishing frequency (see Ref. [14]), which results in finite conductivity $\sigma_{\rm dc}\neq0$ at $\omega\rightarrow0$ [inset of Fig. 2(a)]. This demonstrates conducting behavior in the case of existence of large polarons, corresponding to such small values of χ. Note the difference of a few orders of magnitude in the scale of the system's response in these two frequency regimes (vibrational vs electronic part of the spectrum).

For higher values of the coupling constant χ, corresponding to small polarons, the conductivity shows similar behavior. Again there exist strong peaks at the electronic part of the polaron normal mode spectrum (at even higher frequencies now, cf. Fig. 4 of Ref. [14]), but longer transient times are necessary for reaching the steady state. A qualitative difference appears in the vibrational part of the spectrum, where the lowest frequency polaronic eigenmode now has finite frequency (see the mode labeled "1" in Fig. 4 of Ref. [14], which tends towards the lower edge of the phononic optical band of the PBD model as χ increases) and the response is

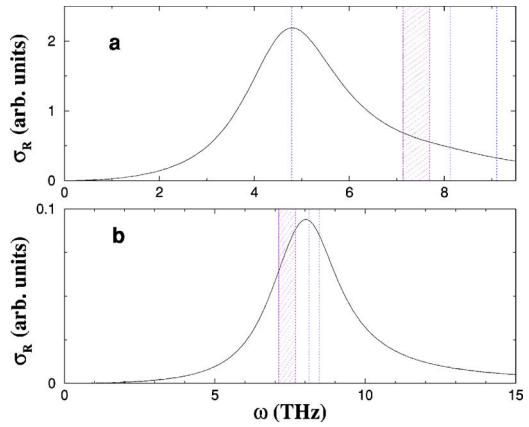

FIG. 3. (Color online) Real part σ_R of the conductivity as a function of frequency for (a) $\chi=1.4$ eV/Å and (b) $\chi=2$ eV/Å, in the vibrational part of the spectrum. The amplitude of the ac field is $E_0=2\times10^{-8}$ V/Å. Vertical dotted lines show the positions of discrete polaronic normal mode frequencies, while the shadowed stripe represents the phononic band of the polaronic normal mode spectrum.

weaker. For example, in Fig. 3(a) we show the real part of the optical conductivity in this regime for $\chi=1.4$ eV/Å. Contrasting with the response shown in the inset of Fig. 2(a), we see that for small polarons the dc conductivity (for $\omega\rightarrow0$) vanishes, resulting in insulating behavior. When χ increases further and the localized polaronic eigenmode "1" enters the phononic optical band, the response in the low frequency part of the spectrum comes from the localized antisymmetric polaronic eigenmode above this band (mode labeled "4" in Fig. 4 of Ref. [14]) and is even weaker [see Fig. 3(b)].

The position of the peaks appearing in the ac response of the system may depend on the amplitude E_0 of the external

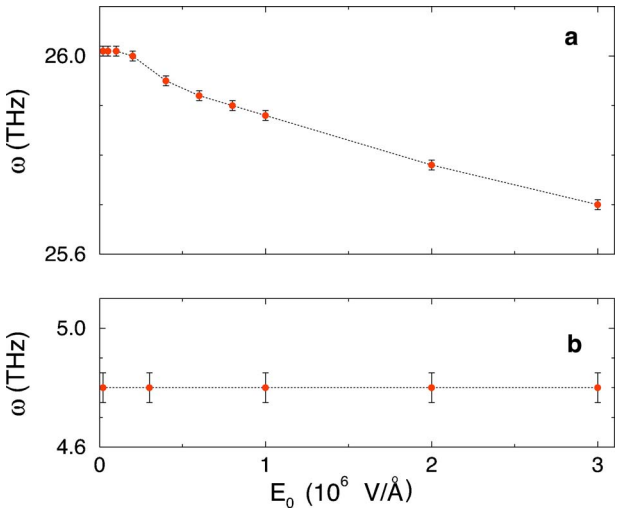

FIG. 4. (Color online) Variation of the frequency of the ac response with the amplitude E_0 of the ac field (8). (a) Redshift of the most prominent peak of $\sigma(\omega)$ for $\chi=0.6$ eV/Å. (b) Absence of redshift for the weaker feature at the vibrational regime for $\chi=1.4$ eV/Å. The errors $\delta\omega$ correspond to the frequency increments used in the calculations. The dotted lines are guides to the eye.

field. In Fig. 4(a) we show that the most prominent peak of $\sigma(\omega)$ for $\chi=0.6$ eV/Å (the case shown in Fig. 2) moves towards lower frequencies by increasing E_0, thus exhibiting a significant redshift. This mode corresponds to the lowest frequency polaronic eigenmode with primarily electronic character. As can be seen from Fig. 2, the redshifts of the electronic character polaronic normal modes depend on the particular peak and it seems that they are more pronounced for higher frequencies. On the contrary, such a redshift is absent for the weaker vibrational peak at $\chi=1.4$ eV/Å [case shown in Fig. 3(a)], as can be seen in Fig. 4(b).

In summary, our calculations show peaks of the ac conductivity at (i) many antisymmetric polaron normal modes with electronic character (the dominant features of the ac spectrum at relatively high frequencies) and (ii) a single antisymmetric polaronic eigenmode (the lowest-frequency localized eigenmode) in the vibrational part of the spectrum (a much weaker but clearly distinguished feature at lower frequencies). The ac-field "active" eigenmodes determined here, combined with the known dependence of the whole polaronic normal mode spectrum on the coupling parameter χ [14] (the only parameter of the model where no estimate of its value is currently available), allows the prediction of the ac response of the system for any value of χ.

The calculation of experimentally measured quantities, such as the ac conductivity presented here or the diffusion coefficient reported in Ref. [28], allows direct tests of our coupled charge-lattice model. In view of the many different charge-vibrational models that have been proposed for charge transport in DNA [11,13,16,29,30], such an evaluation is necessary to determine the principle structural degrees of freedom coupled to charge motion.

Research at Los Alamos National Laboratory is performed under the auspices of the U.S. Department of Energy (Contract No. W-7405-ENG-36).

[1] S. O. Kelley and J. K. Barton, Science **283**, 375 (1999).
[2] Y. A. Berlin, I. V. Kurnikov, D. Beratan, M. A. Ratner, and A. L. Burin, Top. Curr. Chem. **237**, 1 (2004).
[3] R. G. Endres, D. L. Cox, and R. R. P. Singh, Rev. Mod. Phys. **76**, 195 (2004).
[4] C. Dekker and M. A. Ratner, Phys. World **2001**, 29 (2001).
[5] H. W. Fink and C. Schonenberger, Nature (London) **398**, 407 (1999).
[6] D. Porath, A. Bezryadin, S. Vries, and C. Dekker, Nature (London) **403**, 635 (2000).
[7] P. J. Pablo *et al.*, Phys. Rev. Lett. **85**, 4992 (2000).
[8] K.-H. Yoo, D. H. Ha, J.-O. Lee, J. W. Park, J. Kim, J. J. Kim, H.-Y. Lee, T. Kawai, and H. Y. Choi., Phys. Rev. Lett. **87**, 198102 (2001).
[9] H. Böttger and V. V. Bryksin, *Hopping Conduction in Solids* (Akademie-Verlag, Berlin, 1985).
[10] S. S. Alexandre, E. Artacho, J. M. Soler, and H. Chacham, Phys. Rev. Lett. **91**, 108105 (2003).
[11] S. V. Rakhmanova and E. M. Conwell, J. Phys. Chem. B **105**, 2056 (2001).
[12] D. M. Basko and E. M. Conwell, Phys. Rev. E **65**, 061902 (2002).
[13] S. Komineas, G. Kalosakas, and A. R. Bishop, Phys. Rev. E **65**, 061905 (2002).
[14] P. Maniadis, G. Kalosakas, K. Ø. Rasmussen, and A. R. Bishop, Phys. Rev. B **68**, 174304 (2003).
[15] G. Kalosakas, K. Ø. Rasmussen, and A. R. Bishop, J. Chem. Phys. **118**, 3731 (2003); Synth. Met. **141**, 93 (2004).
[16] D. Hennig, Eur. Phys. J. B **30**, 211 (2002).
[17] D. Hennig, J. F. R. Archilla, and J. Agarwal, Physica D **180**, 256 (2003).
[18] C. H. Choi, G. Kalosakas, K. Ø. Rasmussen, M. Hiromura, A. R. Bishop, and A. Usheva, Nucleic Acids Res. **32**, 1584 (2004).
[19] G. Kalosakas, K. Ø. Rasmussen, A. R. Bishop, C. H. Choi, and A. Usheva, Europhys. Lett. **68**, 127 (2004).
[20] S. Ares, N. K. Voulgarakis, K. Ø. Rasmussen, and A. R. Bishop, Phys. Rev. Lett. **94**, 035504 (2005).
[21] T. Dauxois, M. Peyrard, and A. R. Bishop, Phys. Rev. E **47**, R44 (1993).
[22] P. Tran, B. Alavi, and G. Grüner, Phys. Rev. Lett. **85**, 1564 (2000).
[23] E. Helgren, A. Omerzu, G. Grüner, D. Mihailovic, R. Podgornik, and H. Grimm, cond-mat/0111299 (unpublished).
[24] N. P. Armitage, M. Briman, and G. Grüner, Phys. Status Solidi B **241**, 69 (2004).
[25] Z. G. Yu and X. Song, Phys. Rev. Lett. **86**, 6018 (2001).
[26] G. P. Triberis, C. Simserides, and V. C. Karavolas, J. Phys.: Condens. Matter **17**, 2681 (2005).
[27] A. Hübsch, R. G. Endres, D. L. Cox, and R. R. P. Singh, Phys. Rev. Lett. **94**, 178102 (2005).
[28] G. Kalosakas, K. L. Ngai, and S. Flach, Phys. Rev. E **71**, 061901 (2005).
[29] A. Troisi and G. Orlandi, J. Phys. Chem. B **106**, 2093 (2002).
[30] A. Omerzu, M. Licer, T. Mertelj, V. V. Kabanov, and D. Mihailivic, Phys. Rev. Lett. **93**, 218101 (2004).